CRYSTAL GROWTH & DESIGN

pubs.acs.org/crystal

Article

Embroidering Ionic Cocrystals with Polyiodide Threads: The Peculiar Outcome of the Mechanochemical Reaction between Alkali Iodides and Cyanuric Acid

Simone d'Agostino,* Oleksii Shemchuk, Paola Taddei,* Dario Braga, and Fabrizia Grepioni

Cite This: *Cryst. Growth Des.* 2022, 22, 2759–2767

Read Online

ACCESS | Metrics & More | Article Recommendations | Supporting Information

ABSTRACT: We report here the preparation and structural characterization of a series of new crystalline materials obtained by mechanochemical mixing of cyanuric acid (CA) and alkali halides (LiI, NaI, and KI) in the presence of molecular iodine, namely, the isomorphous *catena*-poly[*tetra*(cyanuric acid)·lithium tetraiodide], $n[CA_4{\cdot}LiI_4]$, and *catena*-poly[*tetra*(cyanuric acid)·sodium tetraiodide], $n[CA_4{\cdot}NaI_4]$, featuring three-dimensional (3D) cationic frameworks able to segregate linear, infinite $n[I_4^-]$ chains in their squared open channels and the layered solid $[CA{\cdot}KI_3]_2{\cdot}I_2{\cdot}2H_2O$ characterized by alternating sheets of (i) hydrated potassium cations and CA molecules and (ii) I_3^- anions and discrete I_2 molecules. The combination of X-ray diffraction (XRD), Raman spectroscopy, and thermal analyses allowed us to elucidate the compound's structural features and to discuss the effect of cation size on the stoichiometry and architecture of the three ionic cocrystals (ICCs).

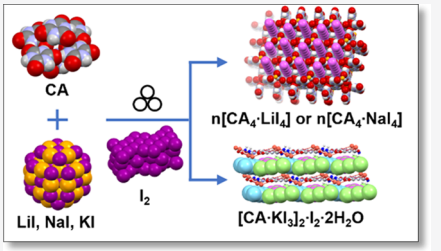

INTRODUCTION

Polyiodides are defined as polyhalogenated anionic species that can be regarded as combinations of I_2, I^-, and I_3^- units.[1,2] In most cases, polyiodides can be described with the general formula I_{2m+n}^{n-}, in which *n* and *m* represent the number of iodide anions (I^-) and of iodine molecules (I_2), respectively.[3,4]

In the solid state, polyiodides display a vast diversity of compositions and structures, ranging from the simplest and linear I_3^- and I_4^{2-} to the V-shaped I_5^- and zigzag I_{23}^{3-} anions, complex two-dimensional (2D) networks, and three-dimensional (3D) cage-like structures, such as I_9^- and I_7^-; infinite polyiodide homopolymers $I_\infty^{\delta-}$ have also been reported.[4−8] The structural diversity of polyiodides is a consequence of the ability of I_2 to catenate through I···I interactions with I^- and I_3^- anions.[9−11]

The general preparation method of polyiodides relies on the addition of stoichiometric amounts of I_2 to a compound containing I^- or I_3^- in a suitable reaction medium, usually a liquid. Though simple, this procedure can be varied in many ways depending on the solvent used and on the nature and size of the cation associated with the iodide or triiodide anion.[3]

As a rule of thumb, large cations favor the formation of extended polyiodide chains in the solid state,[3,4,12] and various supramolecular interactions such as hydrogen or halogen bonds,[11,13−15] caging,[16,17] and anion···π[18,19] concur to stabilize the chains within the crystalline material.[2]

Polyiodides, though extensively studied, constitute a class of materials still relatively poorly understood, and their intrinsic structural unpredictability has prompted further research in this direction,[20] in particular, to rationalize the formation of polyiodide infinite chains, which are, in turn, sought for their potential applications as electrolytes in solar cells,[21−24] electrochemical devices,[25−27] and optical devices,[26,28] among others.

Linear polyiodide infinite chains are a rare subset of polyiodide infinite chains, and, to date, only a limited number of examples has been reported;[4,20,29−32] for this reason, the focus of the current research in the field is the systematic investigation of synthetic methodologies able to produce and control such structural arrangements.

Recently, we have demonstrated, using crystal engineering principles[33,34] and mechanochemical methods,[35,36] that cyanuric acid (CA) is able to form ionic cocrystals (ICCs)[58] with a variety of alkali halides (MX).[37,38] Recently, ICCs with LiCl have also found applications as a solar-blind nonlinear optical material.[55]

In this work, we show how the affinity of cyanuric acid for alkali halides, and their solid-state reactivity toward iodine, can be exploited for the mechanochemical preparation of polyiodide-containing crystalline materials. To this end, we have deliberately added solid iodine, I_2, to solid mixtures of cyanuric acid and the alkali iodides LiI, NaI, and KI. As a result, three novel ionic cocrystals (ICCs) have been obtained, namely, the isomorphous *catena*-poly[*tetra*(cyanuric acid)·lithium tetraiodide], $n[CA_4{\cdot}LiI_4]$, and *catena*-poly-

Received: February 16, 2022
Revised: March 8, 2022
Published: March 16, 2022

https://doi.org/10.1021/acs.cgd.2c00202
Cryst. Growth Des. 2022, 22, 2759−2767

[*tetra*(cyanuric acid)·sodium tetraiodide], $n[CA_4{\cdot}NaI_4]$, both featuring a 3D cationic framework able to segregate linear, infinite $n[I_4^-]$ chains in its squared open channels, and the layered solid $[CA{\cdot}KI_3]_2{\cdot}I_2{\cdot}2H_2O$, characterized by alternating sheets of (i) hydrated potassium cations and CA molecules and (ii) I_3^- anions and discrete I_2 molecules. All compounds have been characterized by a combination of single-crystal and variable-emperature powder X-ray diffraction (XRD), thermogravimetry, hot-stage microscopy, and Raman spectroscopy.

EXPERIMENTAL SECTION

Synthesis. *Materials.* All reagents were purchased from Sigma-Aldrich and used without further purification. Distilled water and reagent-grade solvents were used.

Mechanochemical Synthesis of $n[CA_4{\cdot}LiI_4]$, $n[CA_4{\cdot}NaI_4]$, and $[CA{\cdot}KI_3]_2{\cdot}I_2{\cdot}2H_2O$. Polycrystalline products were obtained by kneading the reactants, weighed in the proper stoichiometric ratio (see Table 1), in the presence of a few drops (ca. 0.1 mL) of methanol for 60 min in a ball-milling apparatus Retsch MM 20 operating at 20 Hz, equipped with an agate jar and two agate balls with a diameter of 5 mm.

Table 1. Amounts of Reagents Used in the Mechanochemical Synthesis of $n[CA_4{\cdot}LiI_4]$, $n[CA_4{\cdot}NaI_4]$, and $[CA{\cdot}KI_3]_2{\cdot}I_2{\cdot}2H_2O$

product	MI[a] (mg; mmol)	CA (mg; mmol)	I_2 (mg; mmol)
$n[CA_4{\cdot}LiI_4]$	84; 0.45	231; 1.80	170; 0.67
$n[CA_4{\cdot}NaI_4]$	61; 0.33	170; 1.33	125; 0.50
$[CA{\cdot}KI_3]_2{\cdot}I_2{\cdot}2H_2O$	78; 0.47	60; 0.46	180; 0.70

[a] $LiI{\cdot}3H_2O$; $NaI{\cdot}2H_2O$; KI.

Solution Synthesis. Cyanuric acid (CA) (60 mg (0.46 mmol)) was suspended in ca. 30 mL of methanol, and then 0.11 mmol of $LiI{\cdot}3H_2O$ (21 mg), $NaI{\cdot}H_2O$ (21 mg), or KI (19 mg) was added in separate preparations. The resulting mixture was kept stirring at RT overnight until a clear solution was obtained. The solution was filtered to remove the unreacted material, refluxed for ca. 6 h, and then cooled to RT. A slight excess of solid iodine (ca. 50 mg) was added, and the resulting solution was left to slowly evaporate in the dark. After 1 week, yellow-orange to brown crystals suitable for XRD were obtained, concomitantly to colorless crystals of unreacted cyanuric acid, identified as CYURAC13.[39]

X-ray Diffraction. *Crystal Structure Determination.* Single-crystal data for all compounds were collected at RT on an Oxford X'Calibur S CCD diffractometer equipped with a graphite monochromator (Mo Kα radiation, λ = 0.71073 Å). All of the $n[CA_4{\cdot}LiI_4]$ samples displayed crystal twinning: data were thus treated with the default configuration for twinned crystals of CrysAlisPro, and structure solution and refinement were performed on the HKLF4 file containing the nonoverlapped reflections. All structures were solved by intrinsic phasing with SHELXT[40] and refined on F^2 by full-matrix least-squares refinement with SHELXL[41] implemented in Olex2 software.[42] All non-hydrogen atoms were refined anisotropically; the rigid-body RIGU restraint was applied.[43] H_{CH} atoms for all compounds were added in calculated positions and refined riding on their respective carbon atoms. Data collection and refinement details are listed in Table SI-1. The Mercury[44] program was used to calculate intermolecular interactions and for molecular graphics. Crystal data can be obtained free of charge via www.ccdc.cam.ac.uk/conts/retrieving.html (or from the Cambridge Crystallographic Data Centre, 12 Union Road, Cambridge CB21EZ, U.K.; Fax: (+44)1223-336-033; or Email: deposit@ccdc.cam.ac.uk). CCDC numbers 2150725−2150727.

Powder Diffraction Measurements. For phase identification and variable-temperature X-ray powder diffraction experiments, diffractograms were recorded on a PANalytical X'Pert Pro automated diffractometer equipped with an X'Celerator detector in the Bragg−Brentano geometry, using Cu Kα radiation (λ = 1.5418 Å) without monochromator in the 2θ range between 5 and 40° (continuous scan mode, step size 0.0167°, counting time 19.685 s, Soller slit 0.04 rad, antiscatter slit 1/2, divergence slit 1/4, 40 mA 40 kV), and an Anton-Paar TTK 450 + LNC. The program Mercury[44] was used for the calculation of the X-ray powder patterns based on single-crystal data either retrieved from the Cambridge structural database (CSD),[45] the Inorganic Crystal Structure Database (ICSD),[46] or collected in this work.

Thermal Characterization. *Thermogravimetric Analysis.* TGA measurements on all samples were performed with a PerkinElmer TGA7 thermogravimetric analyzer, in the 30−400 °C temperature range, under a N_2 gas flow and at a heating rate of 5.00 °C min^{-1}.

Hot-Stage Optical Microscopy. The analyses were carried out using a microscope OLYMPUS BX41 equipped with a NIKON DS FI3 camera. For the temperature control, a Linkam TMS94 stage was used. Images and movies were recorded with a 100× magnification.

Raman Spectroscopy. *Micro-Raman Spectroscopy.* Spectra for single crystals of $n[CA_4{\cdot}LiI_4]$, before and after thermal treatment at 300 °C, and of $[CA{\cdot}KI_3]_2{\cdot}I_2{\cdot}2H_2O$ were obtained using an NRS-2000C (Jasco International Co., Ltd. Tokyo, Japan) instrument with a microscope of 10× magnification. All of the spectra were recorded under backscattering conditions with a 5 cm^{-1} spectral resolution using the 532 nm green diode-pumped solid-state laser driver (RgBLase LLC, Fremont, CA) with a power of about 1 mW to avoid sample degradation. A 160 K cooled digital charge-coupled device (Spec-10: 100B, Roper Scientific, Inc., Sarasota, FL) was used as a detector.

Raman Spectroscopy. Due to the high fluorescence background observed at a 532 nm excitation wavelength, the spectrum of thermally treated $[CA{\cdot}KI_3]_2{\cdot}I_2{\cdot}2H_2O$ powder was recorded on a Bruker MultiRam FT-Raman spectrometer equipped with a cooled Ge-diode detector. The excitation source was a Nd^{3+}-YAG laser (1064 nm) in the backscattering (180°) configuration. The focused laser beam diameter was about 100 μm, and the spectral resolution was 4 cm^{-1}. The laser power at the sample was about 10 mW. The spectrum of cyanuric acid was recorded for comparison.

RESULTS AND DISCUSSION

Synthesis and Structural Characterization of the ICCs $n[CA_4{\cdot}LiI_4]$, $n[CA_4{\cdot}NaI_4]$, and $[CA{\cdot}KI_3]_2{\cdot}I_2{\cdot}2H_2O$. Bulk samples of $n[CA_4{\cdot}LiI_4]$ could be obtained by solution synthesis (see the Experimental Section), but traces of cyanuric acid were invariably present in the solid product. This can be explained by the large differences in solubility between the reactants as CA is only slightly soluble in methanol and tends to crystallize before the desired product. Slow solvent evaporation and change of solvent invariably failed to yield a pure polycrystalline sample; however, methanol remained the best solvent of choice. The solution to the product purity problem could be found in mechanochemistry: the reactants were ground together in the presence of a few drops of methanol, and pure polycrystalline $n[CA_4{\cdot}LiI_4]$ was obtained (see the SI for a comparison of powder diffraction patterns). The same synthetic strategy was extended to sodium and potassium iodides, and analogous mechanochemical reactions were performed with $NaI{\cdot}2H_2O$ and KI. As shown by the powder XRD patterns recorded on the solid products, in both cases, the presence of a new phase, different from the starting materials, can be detected (see Figures 1 and SI-2). In the case of sodium iodide, the pattern obtained very much resembles that obtained with lithium iodide, thus indicating that the two solids are likely to be isomorphous. In the case of potassium iodide, however, the resulting pattern differs considerably from that observed for lithium and sodium, and the presence of

https://doi.org/10.1021/acs.cgd.2c00202
Cryst. Growth Des. 2022, 22, 2759−2767

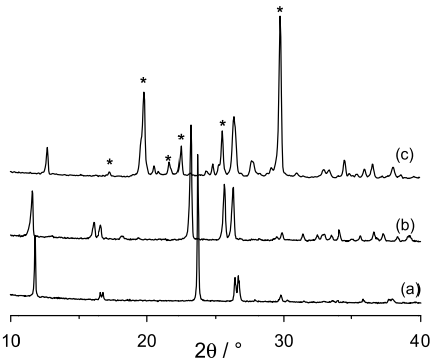

Figure 1. Powder XRD pattern comparison between the products obtained via kneading with MeOH in the solids MI, CA, and I_2 in a 1:4:1.5 stoichiometric ratio; (a) $n[CA_4{\cdot}LiI_4]$, MI = $LiI{\cdot}3H_2O$, (b) $n[CA_4{\cdot}NaI_4]$, MI = $NaI{\cdot}2H_2O$, and (c) $[CA{\cdot}KI_3]_2{\cdot}I_2{\cdot}2H_2O$, MI = KI [asterisks indicate the peaks of unreacted CA (CSD refcode: CYURAC13)].

unreacted cyanuric acid indicates a different stoichiometric ratio.

Single crystals for structural characterization were obtained in the case of lithium by the addition of an equimolar amount of I_2 to a reactive mixture of cyanuric acid (CA) and lithium iodide in methanol, followed by slow solvent evaporation; a small number of yellow-orange crystals of $n[CA_4{\cdot}LiI_4]$ (see Figure 2) could be recovered amidst the bulk of colorless CA crystals.

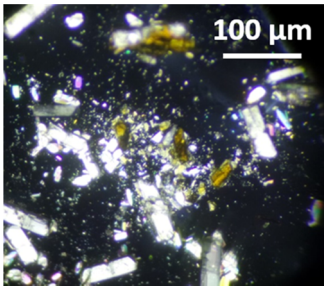

Figure 2. Optical microscopic image taken under polarized light, showing yellow-orange crystals of $n[CA_4{\cdot}LiI_4]$ among the colorless crystals of cyanuric acid.

The same solution procedure applied to sodium and potassium iodides yielded tiny brown/yellowish single crystals of $n[CA_4{\cdot}NaI_4]$ and brown single crystals of $[CA{\cdot}KI_3]_2{\cdot}I_2{\cdot}2H_2O$ (see the Experimental Section).

The two ionic cocrystals obtained with lithium and sodium iodides are isomorphous and will be described together.

In crystalline $n[CA_4{\cdot}LiI_4]$, the cyanuric acid molecules are coordinated to the lithium cations [$Li^+{\cdots}O_{CA}$ distances 1.887(4), 2.096(4), and 2.590(4) Å] in a distorted octahedral geometry (see Figure 3a); the $Li^+{\cdots}O_{CO}$ distance evidenced in blue in the figure is longer than the values commonly observed for oxygen coordination to lithium; an inspection of the anisotropic displacement parameter of the lithium cation, however, shows a "frustrated" lithium-ion position along the −CO···Li^+···OC− direction, as the lithium ion is likely to be statistically closer to only one of the two −CO groups, but its position is averaged on the total number of unit cells in the crystal. In the sodium analogue, on the contrary, the larger sodium cation is more tightly accommodated inside a less distorted octahedron of O_{CO} atoms [$Na^+{\cdots}O$ distances 2.187(1) and 2.540(7) Å], and its anisotropic displacement parameters are close to those of a sphere (see Figure 3b).

Crystalline $n[CA_4{\cdot}LiI_4]$ consists of 2D cationic layers, parallel to the *ab*-plane, formed by the lithium cations and the cyanuric acid molecules (see Figure 4a). The cyanuric acid −C═O and −NH groups protruding from the 2D layer surface (see Figure 4b) act as a hydrogen-bonding glue to adjacent layers above and below the plane [$N(H)_{CA}{\cdots}O_{CA}$ distances in the range of 2.753(7)−2.986(8) Å]; this results in the formation of a 3D cationic network with square-section channels (see Figure 5a) that host the $n[I_4^-]$ polyiodide chains, as shown in Figure 5b. Analogous arrangement is found in the isomorphous ICC $n[CA_4{\cdot}NaI_4]$.

The channels run parallel to the crystallographic *c*-axis and possess an internal diameter of ca. 7 Å; the infinite linear polyiodide chains $n[I_4^-]$ hosted in the channels are characterized by an equidistant arrangement of iodine/iodide [I···I distances 3.008(1) and 3.013(2) Å; $I{-}I{-}I_{angle}$ = 180°] (see Figure 6). In the crystalline $n[CA_4{\cdot}NaI_4]$, the same linear chain is found, with I···I distances of 2.998(3) and 3.000(3) Å.

The $I^-{\cdots}I^-$ van der Waals distance of ca. 4.3 Å is much longer than the ca. 3.01 Å I···I distance observed in crystalline $n[CA_4{\cdot}LiI_4]$, which, in turn, is slightly longer than the I···I distance of ca. 2.8 Å present in perturbed I_2 units.[47,48]

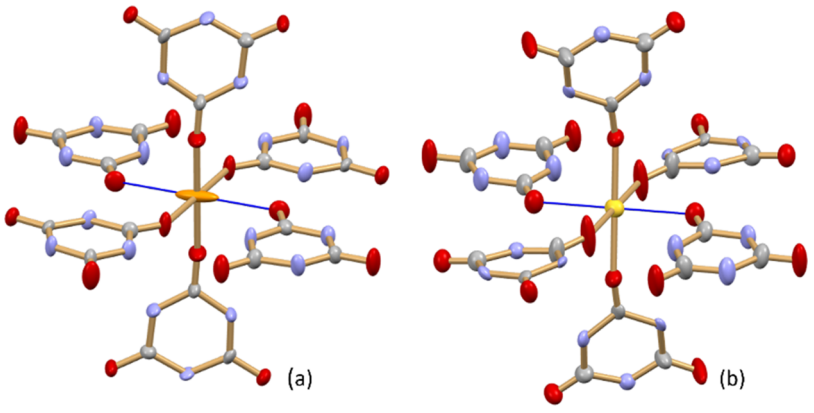

Figure 3. Distorted octahedral coordination of cyanuric acid molecules around the lithium (a) and sodium (b) cations in the ionic cocrystals $n[CA_4{\cdot}LiI_4]$ and $n[CA_4{\cdot}NaI_4]$, respectively. Note the "frustration" of the lithium-ion position along the −CO···Li^+···OC− direction (in blue) evidenced by the lithium-ion anisotropic displacement parameters. H atoms are not shown for clarity.

https://doi.org/10.1021/acs.cgd.2c00202
Cryst. Growth Des. 2022, 22, 2759−2767

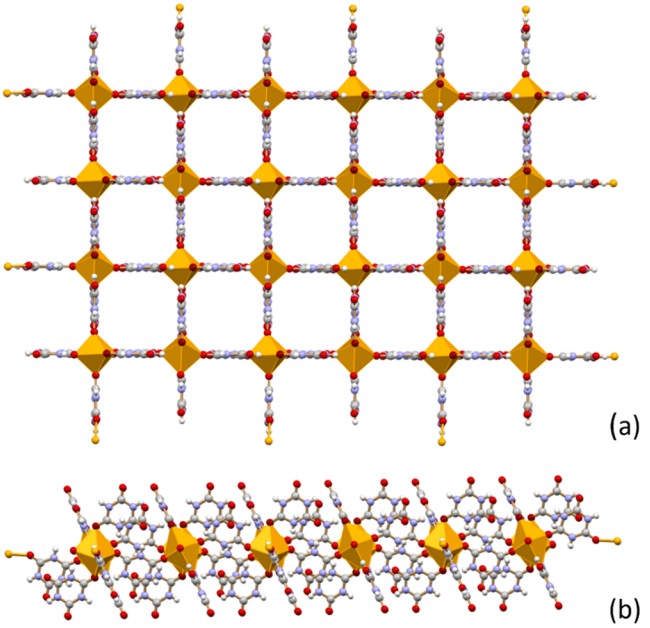

Figure 4. 2D network in crystalline $n[CA_4{\cdot}LiI_4]$ formed via complexation of the lithium cations by cyanuric acid: six O_{CO} atoms belonging to six CA molecules are arranged in an octahedral geometry (in orange) around each cation. (a) View of one 2D layer in the crystallographic *ab*-plane and (b) side view of the same layer. The −CO and −NH groups protruding from both sides of the layer are available for the formation of hydrogen bonds of the −N−H···O═C type, with layers immediately above and below the plane.

Polyiodides are usually described as $(I_3^-\cdots I_2)_n$ or $(I_2\cdots I^-\cdots I_2)_n$ modules of alternating I^- or I_3^- donors and the I_2 acceptor[3,49] or as chains of weakly interacting I_3^- discrete units.[4,50] In all of these cases, alternating I···I distances are invariably observed in the crystals; in $n[CA_4{\cdot}LiI_4]$, on the contrary, all distances between iodine centers along the chain are almost identical; this is not due to some refinement artifact, as no disorder along the chain could be detected in the crystal structure except for anisotropic displacement parameters showing elongation along the chain direction, which denotes a sort of positional frustration also for the iodine centers. This prompted us to perform Raman spectroscopy measurements to gain insight into the iodine atom/iodide ion distribution within the channels and collect further evidence of the infinite character of the polyiodide chain (see below).

On passing from Li^+ and Na^+ to the larger cation K^+, a completely different ICC was obtained, with the formula $[CA{\cdot}KI_3]_2{\cdot}I_2{\cdot}2H_2O$. Figure 7a shows the presence of alternating cationic and anionic layers in the crystal. The cationic layers are formed by CA and H_2O molecules coordinated to the potassium cations; hydrogen-bonding interactions are at work within these layers, with carbonyl groups on CA at a short distance to −NH donors on neighboring CA molecules $[N(H)_{CA}\cdots O_{CA}$ = 2.918(6) Å] and to water molecules $[O_{CA}\cdots O_w$ 2.895(7) Å] (see Figure 7b). As usually observed for metal cations in ionic cocrystals, the geometry around the potassium cation is not regular, and K^+ is at a close distance to three cyanuric acid molecules $[K^+\cdots O_{CA}$ in the range of 2.732(5)−2.749(4) Å], a water molecule $[K^+\cdots O_w$ 2.745(4) Å], and three I_3^- anions belonging to the anionic layer $[K^+\cdots I_{triiodide}$ in the range of 3.660(2)−3.900(1) Å]. The anionic layer is formed by I_3^- monoanions and I_2 molecules (see Figure 7c). Each I_3^- anion within the layer is "kept in place" by close interactions with the potassium cations below and above the plane, thus forming a 2D net with cavities filled by iodine molecules.

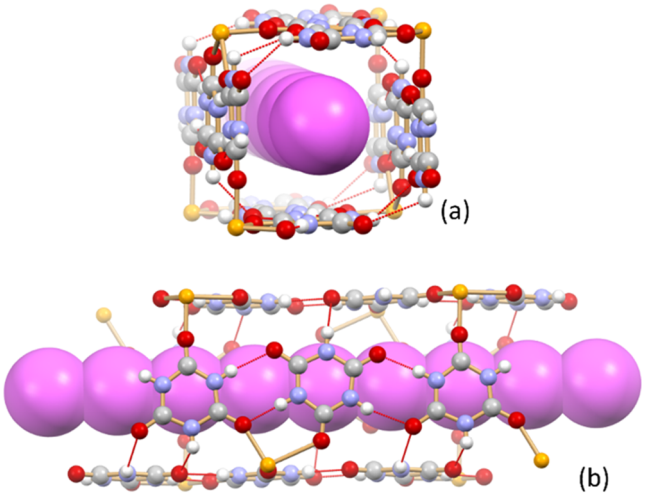

Figure 6. Top (a) and side (b) views of the infinite linear polyiodide chains $n[I_4^-]$ hosted in the channels of crystalline $n[CA_4{\cdot}LiI_4]$ (and in isomorphous $n[CA_4{\cdot}NaI_4]$) are characterized by an equidistant arrangement of iodine/iodide (see the text). Li^+ ions are shown in orange.

Thermal Behavior of $n[CA_4{\cdot}LiI_4]$, $n[CA_4{\cdot}NaI_4]$, and $[CA{\cdot}KI_3]_2{\cdot}I_2{\cdot}2H_2O$. The thermal behavior of $n[CA_4{\cdot}LiI_4]$ and $[CA{\cdot}KI_3]_2{\cdot}I_2{\cdot}2H_2O$ was also investigated to evaluate the stability of molecular iodine "trapped" inside the respective crystal packings.

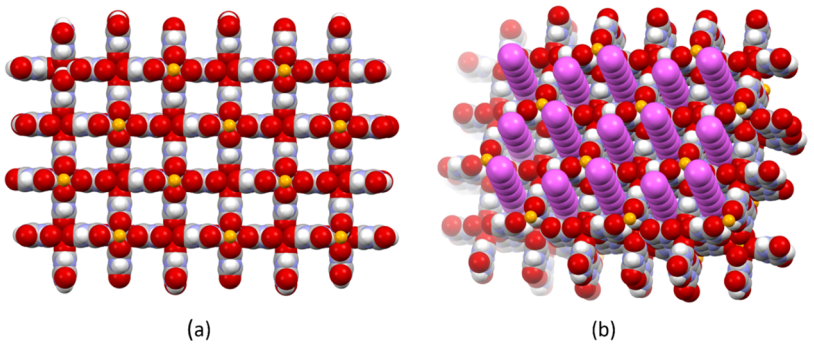

Figure 5. (a) 3D cationic network in crystalline $n[CA_4{\cdot}LiI_4]$ and (b) polyiodide chains filling the cavities along the crystallographic *c*-axis direction [Li^+ orange; I/I^- violet]. The same arrangement is found in the isomorphous ICC $n[CA_4{\cdot}NaI_4]$.

https://doi.org/10.1021/acs.cgd.2c00202
Cryst. Growth Des. 2022, 22, 2759−2767

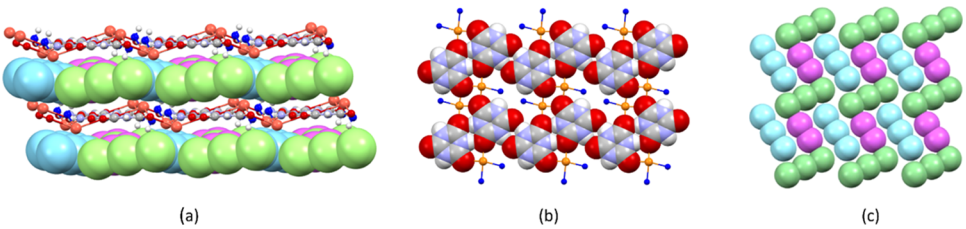

Figure 7. (a) Alternating cationic and anionic layers in crystalline $[CA{\cdot}KI_3]_2{\cdot}I_2{\cdot}2H_2O$. (b) View of the cationic layers showing the hydrogen-bonding pattern of CA molecules and (c) of the anionic layer formed by elemental I_2 (in magenta) and the two crystallographically independent I_3^- anions (in light green and light blue) (K^+ ions are shown in deep orange).

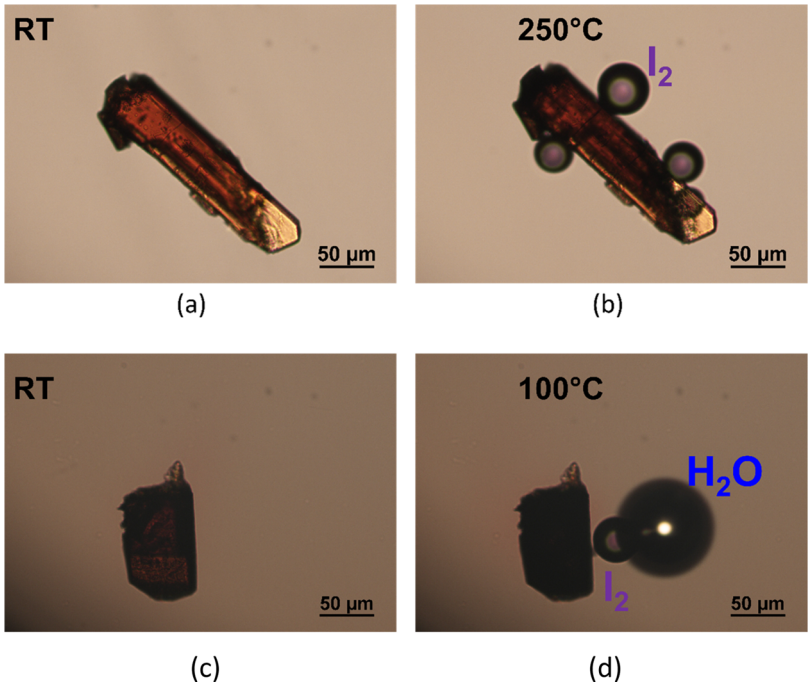

Figure 8. Hot-stage microscopic images taken on single crystals of $n[CA_4{\cdot}LiI_4]$ (a, b) and $[CA{\cdot}KI_3]_2{\cdot}I_2{\cdot}2H_2O$ (c, d) in perfluoropolyether oil. Note the formation of I_2 (b) and I_2/H_2O (d) upon heating.

Scheme 1. Comparison of Thermal Stability toward Iodine Sublimation at Ambient Pressure Between I_2, $n[CA_4{\cdot}LiI_4]$, $n[CA_4{\cdot}NaI_4]$, and $[CA{\cdot}KI_3]_2{\cdot}I_2{\cdot}2H_2O$[a]

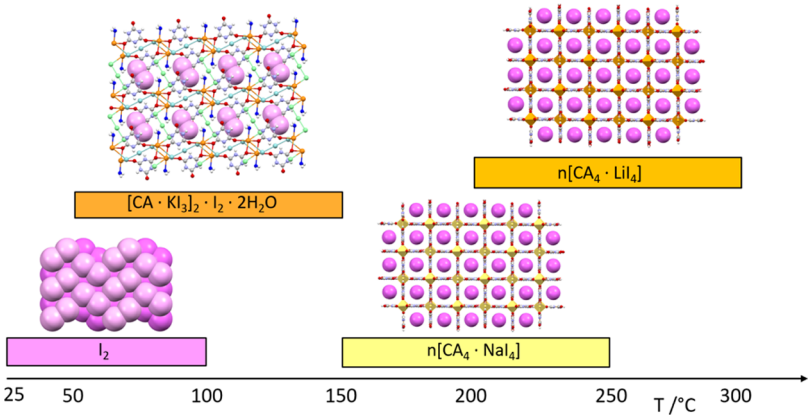

[a]Temperature ranges are taken from TGA measurements (see the SI) at a heating rate of 5 °C min^{-1}.

The TGA trace for $n[CA_4{\cdot}LiI_4]$ (see the SI) shows a first broad event in the temperature range of 200−300 °C due to the loss of approximately 1.5 mol of I_2 per formula unit, followed by degradation. The same process was also investigated by hot-stage microscopy: the release of molecular I_2 is particularly evident around 250 °C (see Figure 8 and movies in the SI). In the presence of perfluoropolyether oil, bubbles of iodine can be observed leaving the crystal from its ends (see movies in the SI), until a colorless solid with a preserved outer shape (see the SI) is obtained, which is no

https://doi.org/10.1021/acs.cgd.2c00202
Cryst. Growth Des. 2022, 22, 2759−2767

longer diffracting. This behavior can be rationalized by considering the relationship between crystal packing and morphology in $n[CA_4{\cdot}LiI_4]$. As demonstrated via face indexing (see Figures SI-6 and SI-7), the channels containing the polyiodide chains run parallel to the crystallographic direction [001], which, in turn, coincides with the direction of maximum growth; therefore, I_2 can flow out of the crystal without stressing the crystal. In the absence of perfluoropolyether oil, iodine leaves the crystals and is condensed on the crystal surface as a black layer; the crystal, at this stage, still diffracts the X-ray radiation, and its channeled structure is maintained. Further removal of iodine from the channels causes disruption of the crystalline edifice, and diffraction is no longer observed.

The TGA trace for $n[CA_4{\cdot}NaI_4]$ shows a first broad event in the temperature range of 150−250 °C due to the loss of approximately 1.5 mol of I_2 per formula unit, followed by degradation. TGA measurements on the potassium ICC $[CA{\cdot}KI_3]_2{\cdot}I_2{\cdot}2H_2O$ show a broad event between 50 and 150 °C, corresponding to the loss of I_2 and H_2O molecules, followed by degradation (see the SI). Hot-stage microscopy evidences the concomitant loss of I_2 and H_2O in the range of 40−150 °C (see Figure 8d), thus confirming the TGA results. A TGA measurement on elemental solid iodine shows that I_2 sublimes in the RT-100 °C range (see the SI). The three ICCs, therefore, show a marked stability increase toward iodine sublimation, as can be seen from a comparison of the iodine release intervals in Scheme 1.

The higher stability for the lithium ICC with respect to the sodium is likely dependent on the higher polarizing effect of lithium toward molecular iodine/iodide chains inside the channels.

Polycrystalline powders of $n[CA_4{\cdot}LiI_4]$ and $[CA{\cdot}KI_3]_2{\cdot}I_2{\cdot}2H_2O$ were finally analyzed by variable-temperature powder XRD. In the case of $n[CA_4{\cdot}LiI_4]$, the loss of molecular iodine, observed upon heating, is accompanied by a loss of crystallinity, already appreciable at 200 °C (see Figure SI-8), and by the appearance of peaks due to pure CA. Upon further heating, at 300 °C, only peaks of CA can be observed (see the SI), and the sample becomes colorless. The behavior of $[CA{\cdot}KI_3]_2{\cdot}I_2{\cdot}2H_2O$ is different, as the loss of I_2/H_2O is accompanied by a phase transformation into a yellow, new crystalline powder, that, as confirmed by the Raman section (see below), can be formulated as $CA{\cdot}KI_3$. XRD peaks of CA and KI are also visible in the pattern at 160 °C and back to RT (see the SI), likely due to the further loss of I_2, upon standing at a high temperature, from the triiodide contained in $CA{\cdot}KI_3$.

Raman Spectroscopy. One of the best methods to study polyiodide species is Raman spectroscopy,[31,51] especially when combined with XRD techniques. Figure 9 shows the micro-Raman spectrum of an $n[CA_4{\cdot}LiI_4]$ single crystal in the low-wavenumber region, i.e., where I−I modes are reported to fall. The spectral pattern in this range appeared significantly different with respect to pure cyanuric acid (whose spectrum is reported for comparison) for both wavenumber positions and band relative intensities. With respect to the latter aspect, polyiodide moieties appeared to exhibit a resonant Raman signal enhancement at a laser excitation wavelength of 532 nm[4,52] so that it is not surprising that vibrational bands at 109 and 158 cm^{-1} were observed as the strongest of the spectrum of $n[CA_4{\cdot}LiI_4]$. Bands at similar wavenumber positions and with analogous full width at half-maximum were reported for pyrroloperylene−iodine complex,[6] which was found to contain $I_\infty^{\delta-}$ infinite polyiodide chains. These authors identified the

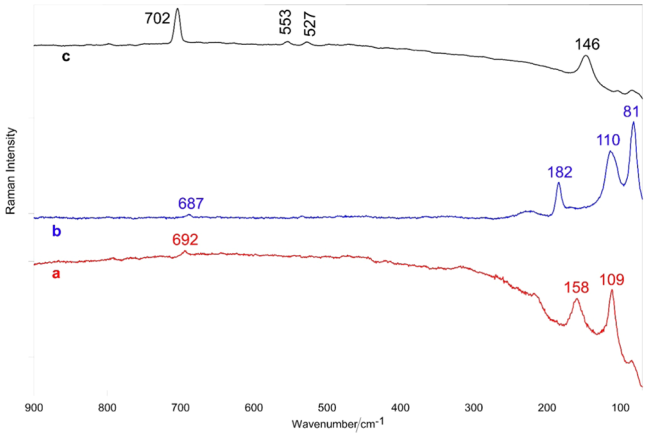

Figure 9. Low-wavenumber Raman spectra of (a) $n[CA_4{\cdot}LiI_4]$ single crystal, (b) $[CA{\cdot}KI_3]_2{\cdot}I_2{\cdot}2H_2O$ single crystal, and (c) cyanuric acid (CA).

above-mentioned Raman bands as characteristic of $I_\infty^{\delta-}$, and based on similarities between their spectrum and the published low-frequency Raman signatures of starch−iodine complex,[53] they inferred the presence of infinite polyiodide chains also in the pyrroloperylene−iodine complex. Actually, finite chains of I_5^-, I_7^-, and I_9^- were found to show bands at higher wavenumber values, i.e., in the 160−180 cm^{-1} range,[31,54] while I_2 has a characteristic band at about 180 cm^{-1}.[31] The absence of the latter spectral features implies that the polymeric polyiodide chain forms a real $I_\infty^{\delta-}$ entity,[4] in agreement with XRD data, rather than extended donor (e.g., I^- or I_3^-)−I_2 acceptor adducts.[49] On the other hand, some authors have observed bands at similar wavenumber positions to ours for very asymmetric triiodides,[56] with a ratio of 1.65 between the wavenumber positions of the vibrational high- and low-energy stretching modes (at 165 and 100 cm^{-1}, respectively). According to Kalina et al.,[57] this value was interpreted as diagnostic for very asymmetric triiodides.[56] In our case, this hypothesis may be excluded on the basis of the XRD results, which showed almost identical distances between iodine centers along the chain. Moreover, it must be stressed that the above-mentioned ratio was only 1.4, i.e., significantly lower than that reported for very asymmetric triiodides. The band at 692 cm^{-1} is assignable to the ring out-of-plane bending vibration of cyanuric acid.[55] This band, which is the strongest in the spectrum of the ligand (Figure 9), was observed as a weak spectral feature in the spectrum of $n[CA_4{\cdot}LiI_4]$; moreover, it appeared shifted with respect to pure cyanuric acid (702 cm^{-1}), according to a trend previously reported in cyanuric acid−melamine adducts.[55] Upon heating at 300 °C, the bands below 200 cm^{-1} significantly decreased in relative intensity, consistently with iodine loss (Figure SI-10); the bands observed in the spectrum are consistent with the presence of cyanuric acid, in agreement with XRD results.

The micro-Raman spectrum in the low-wavenumber region of a $[CA{\cdot}KI_3]_2{\cdot}I_2{\cdot}2H_2O$ single crystal is shown in Figure 9. The observed pattern confirms the structural data, being consistent with the presence of a substantially unperturbed I_2 molecule, band at 182 cm^{-1},[31] and symmetrical linear triiodide, band at 110 cm^{-1}.[31,54] The slight asymmetry of the latter band could account for the presence of two nonequivalent triiodide ions, as detected by single-crystal XRD. Also, in this case, the ring out-of-plane bending vibration of cyanuric acid was detected (687 cm^{-1}).

https://doi.org/10.1021/acs.cgd.2c00202
Cryst. Growth Des. 2022, 22, 2759−2767

Figure SI-11 shows the FT-Raman spectra of the polycrystalline product obtained after variable-temperature PXRD (thermal treatment) of $[CA{\cdot}KI_3]_2{\cdot}I_2{\cdot}2H_2O$, and pure cyanuric acid, reported for comparison. The bands at 1727, 703, and 553 cm^{-1} confirmed the presence of cyanuric acid already detected by XRD. The other spectral features are consistent with $CA{\cdot}KI_3$. In the low-wavenumber range, no band around 180 cm^{-1} was observed, suggesting the absence of unperturbed I_2 building blocks and confirming the I_2 loss disclosed by XRD. The band at about 110 cm^{-1}, assignable to linear symmetrical triiodide,[31,54] was split into two components at 116 and 104 cm^{-1}. The strongest spectral feature below 200 cm^{-1} appeared at 154 cm^{-1}; this band can be due to a perturbed diiodine molecule in a more asymmetric triiodide unit (i.e., $I^-{\cdots}I_2$ adduct).[49,51,54] Going from cyanuric acid to $CA{\cdot}KI_3$, the ring out-of-plane bending vibration shifted to a lower wavenumber value (i.e., 689 cm^{-1}), as previously observed for $n[CA_4{\cdot}LiI_4]$. On the contrary, the mixed mode at 526 cm^{-1} (C═O in-plane bending + side-chain in-plane C−N bending[55]) shifted to higher wavenumbers (i.e., 534 cm^{-1}) and significantly strengthened. As expected, the C═O stretching band shifted from 1727 to 1765 cm^{-1} due to metal coordination.

CONCLUSIONS

In this work, we have reported the preparation and structural characterization by XRD methods and Raman spectroscopy, as well as the investigation of the thermal stability of three novel ionic cocrystals (ICCs) obtained by reacting a series of alkali iodides (MI, with M^+ = Li^+, Na^+, and K^+) with cyanuric acid and in the presence of molecular I_2, namely, $n[CA_4{\cdot}LiI_4]$, $n[CA_4{\cdot}NaI_4]$, and $[CA{\cdot}KI_3]_2{\cdot}I_2{\cdot}2H_2O$.

Mechanochemistry turned out to be essential to quantitatively prepare polycrystalline samples of such hybrid organic−inorganic materials, whose components show extreme solubility differences. Crystalline $n[CA_4{\cdot}LiI_4]$ and $n[CA_4{\cdot}NaI_4]$ are isomorphous and feature the presence of a 3D cationic framework able to segregate and stabilize linear, infinite $n[I_4^-]$ chains in its squared open channels, whereas the crystal structure of $[CA{\cdot}KI_3]_2{\cdot}I_2{\cdot}2H_2O$ consists of a layered solid characterized by alternating sheets of hydrated potassium cations and CA molecules and I_3^- anions and discrete I_2 molecules. The Raman spectral patterns observed in the low-wavenumber range were consistent with the structural features determined by XRD, confirming the usefulness of Raman spectroscopy as an investigation tool of polyiodide-containing systems.

Thermal features of the materials have also been studied; between the two isomorphous ICCs, $n[CA_4{\cdot}LiI_4]$ shows a marked stability increase toward iodine sublimation that can be likely ascribed to the higher polarizing effect of lithium toward molecular iodine/iodide chains inside the channels, whereas the behavior of $[CA{\cdot}KI_3]_2{\cdot}I_2{\cdot}2H_2O$ is different, as loss of I_2/H_2O is accompanied by a phase transformation into a new crystalline powder, which, as confirmed by Raman, has been formulated as $CA{\cdot}KI_3$.

These findings complement our previous results with cyanuric acid and alkali halides with smaller anions[37,38] and further demonstrate the versatility of cyanuric acid in the formation of complex architectures.

Further research is ongoing to extend the same synthetic approach to earth-alkali iodides and to explore the opportunity to obtain novel supramolecular structures that stabilize polyiodide systems.

ASSOCIATED CONTENT

Supporting Information

The Supporting Information is available free of charge at https://pubs.acs.org/doi/10.1021/acs.cgd.2c00202.

X-ray crystallographic data for $n[CA_4{\cdot}LiI_4]$, $n[CA_4{\cdot}NaI_4]$, and $[CA{\cdot}KI_3]_2{\cdot}I_2{\cdot}2H_2O$; additional PXRD patterns (including variable-temperature measurements), TGA traces, face indexing, crystal morphology, and additional Raman spectra; and X-ray crystallographic data for $n[CA_4{\cdot}LiI_4]$, $n[CA_4{\cdot}NaI_4]$, and $[CA{\cdot}KI_3]_2{\cdot}I_2{\cdot}2H_2O$ (PDF)

Movie recorded under the HSM for $n[CA_4{\cdot}LiI_4]$ (MP4)

Movie recorded under the HSM for $[CA{\cdot}KI_3]_2{\cdot}I_2{\cdot}2H_2O$ (MP4)

Accession Codes

CCDC 2150725−2150727 contain the supplementary crystallographic data for this paper. These data can be obtained free of charge via www.ccdc.cam.ac.uk/data_request/cif, or by emailing data_request@ccdc.cam.ac.uk, or by contacting The Cambridge Crystallographic Data Centre, 12 Union Road, Cambridge CB2 1EZ, UK; fax: +44 1223 336033.

AUTHOR INFORMATION

Corresponding Authors

Simone d'Agostino − *Department of Chemistry "Giacomo Ciamician", University of Bologna, 40126 Bologna, Italy;* orcid.org/0000-0003-3065-5860; Email: simone.dagostino2@unibo.it

Paola Taddei − *Department of Biomedical and Neuromotor Sciences, University of Bologna, 40126 Bologna, Italy;* Email: paola.taddei@unibo.it

Authors

Oleksii Shemchuk − *Institute of Condensed Matter and Nanosciences, 1348 Louvain-la-Neuve, Belgium;* orcid.org/0000-0003-3003-3922

Dario Braga − *Department of Chemistry "Giacomo Ciamician", University of Bologna, 40126 Bologna, Italy;* orcid.org/0000-0003-4162-4779

Fabrizia Grepioni − *Department of Chemistry "Giacomo Ciamician", University of Bologna, 40126 Bologna, Italy;* orcid.org/0000-0003-3895-0979

Complete contact information is available at: https://pubs.acs.org/10.1021/acs.cgd.2c00202

Author Contributions

The manuscript was written through contributions of all authors. All authors have given approval to the final version of the manuscript.

Notes

The authors declare no competing financial interest.

ACKNOWLEDGMENTS

The University of Bologna (RFO scheme) and PRIN 2020 are acknowledged for financial support.

REFERENCES

(1) Küpper, F. C.; Feiters, M. C.; Olofsson, B.; Kaiho, T.; Yanagida, S.; Zimmermann, M. B.; Carpenter, L. J.; Luther, G. W.; Lu, Z.; Jonsson, M.; Kloo, L. Commemorating Two Centuries of Iodine Research: An Interdisciplinary Overview of Current Research. *Angew. Chem., Int. Ed.* **2011**, *50*, 11598−11620.

(2) Savastano, M. Words in Supramolecular Chemistry: The Ineffable Advances of Polyiodide Chemistry. *Dalton Trans.* **2021**, *50*, 1142−1165.
(3) Svensson, P. H.; Kloo, L. Synthesis, Structure, and Bonding in Polyiodide and Metal Iodide-Iodine Systems. *Chem. Rev.* **2003**, *103*, 1649−1684.
(4) Poręba, T.; Świątkowski, M.; Kruszyński, R. Molecular Self-Assembly of 1D Infinite Polyiodide Helices in a Phenanthrolinium Salt. *Dalton Trans.* **2021**, *50*, 2800−2806.
(5) D'Agostino, S.; Braga, D.; Grepioni, F.; Taddei, P. Intriguing Case of Pseudo-Isomorphism between Chiral and Racemic Crystals of Rac- and (S)/(R)2-(1,8-Naphthalimido)-2-Quinuclidin-3-Yl, and Their Reactivity toward I_2, and IBr. *Cryst. Growth Des.* **2014**, *14*, 821−829.
(6) Madhu, S.; Evans, H. A.; Doan-Nguyen, V. V. T.; Labram, J. G.; Wu, G.; Chabinyc, M. L.; Seshadri, R.; Wudl, F. Infinite Polyiodide Chains in the Pyrroloperylene−Iodine Complex: Insights into the Starch−Iodine and Perylene−Iodine Complexes. *Angew. Chem., Int. Ed.* **2016**, *55*, 8032−8035.
(7) Demartin, F.; Deplano, P.; Devillanova, F. A.; Isaia, J. F.; Lippois, V.; Veranilb, G.; Press, P.; York, N. Iodonium Salts *First Example of 1-412 Heptaiodide.* 1993, *2*, 3694 3699.
(8) Tebbe, K.-F.; Buchem, R. Das Bisher Iodreichste Polyiodid: Herstellung Und Struktur von Fc_3I_{29}. *Angew. Chem.* **1997**, *109*, 1403−1405.
(9) Wang, Y.; Xue, Y.; Wang, X.; Cui, Z.; Wang, L. The Stable Polyiodides: Experimental and Theoretical Studies of Formation Mechanism. *J. Mol. Struct.* **2014**, *1074*, 231−239.
(10) Manca, G.; Ienco, A.; Mealli, C. Factors Controlling Asymmetrization of the Simplest Linear I 3- and I 42- Polyiodides with Implications for the Nature of Halogen Bonding. *Cryst. Growth Des.* **2012**, *12*, 1762−1771.
(11) Peuronen, A.; Rinta, H.; Lahtinen, M. N···I Halogen Bonding Supported Stabilization of a Discrete Pseudo-Linear $[I_{12}]^{2-}$ Polyiodide. *CrystEngComm* **2015**, *17*, 1736−1740.
(12) Walbaum, C.; Pantenburg, I.; Junk, P.; Deacon, G. B.; Meyer, G. Bulky Cations and Four Different Polyiodide Anions in $[Lu(DB18c6)(H_2O)3(Thf)_6]_4(I_3)$ $2(I_5)_6(I_8)(I_{12})$. *Z. Anorg. Allg. Chem.* **2010**, *636*, 1444−1446.
(13) Savastano, M.; Martínez-Camarena, Á.; Bazzicalupi, C.; Delgado-Pinar, E.; Llinares, J. M.; Mariani, P.; Verdejo, B.; García-España, E.; Bianchi, A. Stabilization of Supramolecular Networks of Polyiodides with Protonated Small Tetra-Azacyclophanes. *Inorganics* **2019**, *7*, No. 48.
(14) Savastano, M.; Bazzicalupi, C.; García-Gallarín, C.; López De La Torre, M. D.; Bianchi, A.; Melguizo, M. Supramolecular Forces and Their Interplay in Stabilizing Complexes of Organic Anions: Tuning Binding Selectivity in Water. *Org. Chem. Front.* **2019**, *6*, 75−86.
(15) Martínez-Camarena, l.; Savastano, M.; Llinares, J. M.; Verdejo, B.; Bianchi, A.; García-España, E.; Bazzicalupi, C. Stabilization of Polyiodide Networks with Cu(II) Complexes of Small Methylated Polyazacyclophanes: Shifting Directional Control from H-Bonds to I···I Interactions. *Inorg. Chem. Front.* **2020**, *7*, 4239−4255.
(16) Lin, J.; Martí-Rujas, J.; Metrangolo, P.; Pilati, T.; Radice, S.; Resnati, G.; Terraneo, G. Solution and Solid State Synthesis of the Discrete Polyiodide I 73- under Modular Cation Templation. *Cryst. Growth Des.* **2012**, *12*, 5757−5762.
(17) Thomas, J. M. Crystal Engineering: Origins, Early Adventures and Some Current Trends. *CrystEngComm* **2011**, *13*, 4304−4306.
(18) Savastano, M.; Bazzicalupi, C.; García, C.; Gellini, C.; López de La Torre, M. D.; Mariani, P.; Pichierri, F.; Bianchi, A.; Melguizo, M. Iodide and Triiodide Anion Complexes Involving Anion-π Interactions with a Tetrazine-Based Receptor. *Dalton Trans.* **2017**, *46*, 4518−4529.
(19) Giese, M.; Albrecht, M.; Bohnen, C.; Repenko, T.; Valkonen, A.; Rissanen, K. Solid State Anion-π Interactions Involving Polyhalides. *Dalton Trans.* **2014**, *43*, 1873−1880.
(20) Savinkina, E. V.; Golubev, D. V.; Grigoriev, M. S.; Kornilov, A. V. Synthesis and Crystal Structure of Rare-Earth Biuret Complexes with Linear Pentaiodide Ions: Infinite Polyiodide Chains in a Cationic Framework. *J. Mol. Struct.* **2021**, *1227*, No. 129526.
(21) Wu, J.; Lan, Z.; Lin, J.; Huang, M.; Huang, Y.; Fan, L.; Luo, G. Electrolytes in Dye-Sensitized Solar Cells. *Chem. Rev.* **2015**, *115*, 2136−2173.
(22) Bella, F.; Galliano, S.; Falco, M.; Viscardi, G.; Barolo, C.; Grätzel, M.; Gerbaldi, C. Unveiling Iodine-Based Electrolytes Chemistry in Aqueous Dye-Sensitized Solar Cells. *Chem. Sci.* **2016**, *7*, 4880−4890.
(23) Turkevych, I.; Kazaoui, S.; Belich, N. A.; Grishko, A. Y.; Fateev, S. A.; Petrov, A. A.; Urano, T.; Aramaki, S.; Kosar, S.; Kondo, M.; Goodilin, E. A.; Graetzel, M.; Tarasov, A. B. Strategic Advantages of Reactive Polyiodide Melts for Scalable Perovskite Photovoltaics. *Nat. Nanotechnol.* **2019**, *14*, 57−63.
(24) Li, B.; Nie, Z.; Vijayakumar, M.; Li, G.; Liu, J.; Sprenkle, V.; Wang, W. Ambipolar Zinc-Polyiodide Electrolyte for a High-Energy Density Aqueous Redox Flow Battery. *Nat. Commun.* **2015**, *6*, No. 6303.
(25) Weng, G. M.; Li, Z.; Cong, G.; Zhou, Y.; Lu, Y. C. Unlocking the Capacity of Iodide for High-Energy-Density Zinc/Polyiodide and Lithium/Polyiodide Redox Flow Batteries. *Energy Environ. Sci.* **2017**, *10*, 735−741.
(26) Yin, Z.; Wang, Q. X.; Zeng, M. H. Iodine Release and Recovery, Influence of Polyiodide Anions on Electrical Conductivity and Nonlinear Optical Activity in an Interdigitated and Interpenetrated Bipillared-Bilayer Metal-Organic Framework. *J. Am. Chem. Soc.* **2012**, *134*, 4857−4863.
(27) Khanna, S. K.; Yen, S. P. S.; Somoano, R. B.; Chaikin, P. M.; Ma, C. L.; Williams, R.; Samson, S. Effects of Disorder on the Transport Properties of Bis (Tetrathiatetracene)Triiodide. *Phys. Rev. B* **1979**, *19*, 655−663.
(28) Kahr, B.; Freudenthal, J.; Phillips, S.; Kaminsky, W. Herapathite. *Science* **2009**, *324*, 1407.
(29) Savastano, M.; Bazzicalupi, C.; Gellini, C.; Bianchi, A. Infinite Supramolecular Pseudo-Polyrotaxane with Poly[3]Catenane Axle: Assembling Nanosized Rings from Mono- And Diatomic I- and I2 Tectons. *Chem. Commun.* **2020**, *56*, 551−554.
(30) Ozaki, N.; Sakamoto, H.; Nishihara, T.; Fujimori, T.; Hijikata, Y.; Kimura, R.; Irle, S.; Itami, K. Electrically Activated Conductivity and White Light Emission of a Hydrocarbon Nanoring−Iodine Assembly. *Angew. Chem., Int. Ed.* **2017**, *56*, 11196−11202.
(31) Redel, E.; Röhr, C.; Janiak, C. An Inorganic Starch-Iodine Model: The Inorganic-Organic Hybrid Compound $\{(C_4H_{12}N_2)_2[CuII_4](I_2)\}$n. *Chem. Commun.* **2009**, *103*, 2103−2105.
(32) Behrens, U.; Breunig, H. J.; Denker, M.; Ebert, K. H. Iodine Chains in (Me, Sb), I, and Discrete Triiodide Ions in Me, AsI_3. *Angew. Chem., Int. Ed.* **1994**, *33*, 987−989.
(33) Braga, D.; Grepioni, F.; Maini, L.; d'Agostino, S. From Solid-State Structure and Dynamics to Crystal Engineering. *Eur. J. Inorg. Chem.* **2018**, *2018*, 3597−3605.
(34) Braga, D.; Grepioni, F.; Maini, L.; d'Agostino, S. Making Crystals with a Purpose; A Journey in Crystal Engineering at the University of Bologna. *IUCrJ* **2017**, *4*, 369−379.
(35) Braga, D.; Maini, L.; Grepioni, F. Mechanochemical Preparation of Co-Crystals. *Chem. Soc. Rev.* **2013**, *42*, 7638−7648.
(36) James, S. L.; Friščić, T. Mechanochemistry. *Chem. Soc. Rev.* **2013**, *42*, 7494−7496.
(37) Shemchuk, O.; Grepioni, F.; Braga, D. Mechanochemical Preparation and Solid-State Characterization of 1:1 and 2:1 Ionic Cocrystals of Cyanuric Acid with Alkali Halides. *Cryst. Growth Des.* **2020**, *20*, 7230−7237.
(38) Shemchuk, O.; Braga, D.; Maini, L.; Grepioni, F. Anhydrous Ionic Co-Crystals of Cyanuric Acid with LiCl and NaCl. *CrystEngComm* **2017**, *19*, 1366−1369.
(39) Söllradl, S.; Greiwe, M.; Bukas, V. J.; Buchner, M. R.; Widenmeyer, M.; Kandemir, T.; Zweifel, T.; Senyshyn, A.; Günther,

https://doi.org/10.1021/acs.cgd.2c00202
Cryst. Growth Des. 2022, 22, 2759−2767

S.; Nilges, T.; Türler, A.; Niewa, R. Nitrogen-Doping in ZnO via Combustion Synthesis? *Chem. Mater.* **2015**, *27*, 4188−4195.
(40) Sheldrick, G. M. SHELXT - Integrated Space-Group and Crystal-Structure Determination. *Acta Crystallogr., Sect. A: Found. Adv.* **2015**, *71*, 3−8.
(41) Sheldrick, G. M. A Short History of SHELX. *Acta Crystallogr., Sect. A: Found. Crystallogr.* **2008**, *64*, 112−122.
(42) Dolomanov, O. V.; Bourhis, L. J.; Gildea, R. J.; Howard, J. A. K.; Puschmann, H. OLEX2: A Complete Structure Solution, Refinement and Analysis Program. *J. Appl. Crystallogr.* **2009**, *42*, 339−341.
(43) Thorn, A.; Dittrich, B.; Sheldrick, G. M. Enhanced Rigid-Bond Restraints. *Acta Crystallogr., Sect. A: Found. Crystallogr.* **2012**, *68*, 448−451.
(44) Macrae, C. F.; Bruno, I. J.; Chisholm, J. A.; Edgington, P. R.; McCabe, P.; Pidcock, E.; Rodriguez-Monge, L.; Taylor, R.; Van De Streek, J.; Wood, P. A. Mercury CSD 2.0 - New Features for the Visualization and Investigation of Crystal Structures. *J. Appl. Crystallogr.* **2008**, *41*, 466−470.
(45) Groom, C. R.; Bruno, I. J.; Lightfoot, M. P.; Ward, S. C. The Cambridge Structural Database. *Acta Crystallogr., Sect. B: Struct. Sci., Cryst. Eng. Mater.* **2016**, *72*, 171−179.
(46) Hellenbrandt, M. The Inorganic Crystal Structure Database (ICSD)—Present and Future. *Crystallogr. Rev.* **2004**, *10*, 17−22.
(47) Noltemeyer, M.; Saenger, W. X-Ray Studies of Linear Polyiodide Chains in α-Cyclodextrin Channels and a Model for the Starch-Iodine Complex. *Nature* **1976**, *259*, 629−632.
(48) Saenger, W. The Structure of the Blue Starch-Iodine Complex. *Naturwissenschaften* **1984**, *71*, 31−36.
(49) Deplano, P.; Ferraro, J. R.; Mercuri, M. L.; Trogu, E. F. Structural and Raman Spectroscopic Studies as Complementary Tools in Elucidating the Nature of the Bonding in Polyiodides and in Donor-I2 Adducts. *Coord. Chem. Rev.* **1999**, *188*, 71−95.
(50) Kloo, L.; Svensson, P. H.; Taylor, M. J. Investigations of the Poly Iodides $H_3O{\cdot}Ix$ (x = 3, 5 or 7) as Dibenzo-18-Crown-6 Complexes. *J. Chem. Soc., Dalton Trans.* **2000**, *7*, 1061−1065.
(51) Deplano, P.; Devillanova, F. A.; Ferraro, J. R.; Isaia, F.; Lippolis, V.; Mercuri, M. L. On the Use of Raman Spectroscopy in the Characterization of Iodine in Charge-Transfer Complexes. *Appl. Spectrosc.* **1992**, *46*, 1625−1629.
(52) Nour, E. M.; Chen, L. H.; Laane, J. Far-Infrared and Raman Spectroscopic Studies of Polyiodides. *J. Phys. Chem. A* **1986**, *90*, 2841−2846.
(53) Teitelbaum, R. C.; Ruby, S. L.; Marks, T. J. On the Structure of Starch-Iodine. *J. Am. Chem. Soc.* **1978**, *100*, 3215−3217.
(54) Blake, A. J.; Devillanova, F. A.; Gould, R. O.; Li, W. S.; Lippolis, V.; Parsons, S.; Radek, C.; Schröder, M. Template Self-Assembly of Polyiodide Networks. *Chem. Soc. Rev.* **1998**, *27*, 195−205.
(55) Wang, K.; Duan, D.; Wang, R.; Liu, D.; Tang, L.; Cui, T.; Liu, B.; Cui, Q.; Liu, J.; Zou, B.; Zou, G. Pressure-Induced Phase Transition in Hydrogen-Bonded Supramolecular Adduct Formed by Cyanuric Acid and Melamine. *J. Phys. Chem. B* **2009**, *113*, 14719−14724.
(56) van Megen, M.; Reiss, G. J. I_6^{2-} Anion Composed of Two Asymmetric Triiodide Moieties: A Competition between Halogen and Hydrogen Bond. *Inorganics* **2013**, *1*, 3−13.
(57) Kalina, D. W.; Lyding, J. W.; Ratajack, M. T.; Kannewurf, C. R.; Marks, T. J. Bromine as a Partial Oxidant. Oxidation State and Charge Transport in Brominated Nickel and Palladium Bis-(diphenylglyoximates). A Comparison with the Iodinated Materials and Resonance Raman Structure-Spectra Correlation for Polybromides. *J. Am. Chem. Soc.* **1980**, *102*, 7854−7862.
(58) Braga, D.; Grepioni, F.; Shemchuk, O. Organic−inorganic ionic co-crystals: a new class of multipurpose compounds. *CrystEngComm* **2018**, *20*, 2212−2220.

https://doi.org/10.1021/acs.cgd.2c00202
Cryst. Growth Des. 2022, 22, 2759−2767